Materials Chemistry and Physics 138 (2013) 449–453

Contents lists available at SciVerse ScienceDirect

Materials Chemistry and Physics

journal homepage: www.elsevier.com/locate/matchemphys

Materials science communication

Evolution of size and shape of gold nanoparticles during long-time aging

Jenő Gubicza [a,*], János L. Lábár [a,b], Luu Manh Quynh [c], Nguyen Hoang Nam [c], Nguyen Hoang Luong [c,d]

[a] Department of Materials Physics, Eötvös Loránd University, Pázmány Péter s. 1/A., H-1117 Budapest, Hungary
[b] Institute for Technical Physics and Materials Science, Research Centre for Natural Sciences, Hungarian Academy of Sciences, Budapest, Hungary
[c] Center for Materials Science, Faculty of Physics, Hanoi University of Science, Vietnam National University, 334 Nguyen Trai, Hanoi, Vietnam
[d] Nano and Energy Center, Vietnam National University, 334 Nguyen Trai, Hanoi, Vietnam

HIGHLIGHTS

- The initial Au particle size of 2–5 nm increased to 25 nm in one year of storage.
- The main mechanisms of Au particle growth are Ostwald ripening and fusion.
- The initial spherical morphology changed to regular shapes.
- Twin boundaries have an important effect on the evolution of morphology.

ARTICLE INFO

Article history:
Received 12 July 2012
Received in revised form
24 November 2012
Accepted 5 January 2013

Keywords:
Nanostructures
Crystal growth
Electron microscopy (STEM, TEM and SEM)
Aging

ABSTRACT

The evolution of size and shape of gold nanoparticles was studied during long-time aging. The initial particle size of 2–5 nm increased to about 25 nm in one year of storage. It was revealed that the main mechanism of particle growth is Ostwald ripening, however, fusion of particles was also observed. Additionally, while the initial particles have spherical morphology, the grown particles show various shapes such as sphere, bipyramid, decahedron, deca-tetrahedron, triangular plate and rod. Twin boundaries with large frequency of ~5% were detected inside the particles which have an important effect on the evolution of morphology. This study suggests that aging may be a new way of tuning size and shape of gold nanoparticles.

1. Introduction

Metallic particles with dimensions of several nanometers are of great interest due to their unusual behavior. For instance, the optical properties of nanosized metal particles are essentially different from the behavior of bulk materials. An incident light can stimulate collective electron charge oscillations in metallic nanocrystals and a resonance occurs when the frequency of light photons matches the natural frequency of surface electrons oscillating against the restoring force of positive nuclei (localized surface plasmon resonance-LSPR) [1]. Among metallic nanoparticles, Au and Ag nanocrystals are in the focus of interest as their LSPR frequencies usually fall in the range of visible light. For example, gold nanoparticles with the diameter of 3–30 nm appear red when suspended in a transparent media [2]. However, the size and shape of Au nanocrystals, the structure of their surface and the dielectric properties of the medium separating them have considerable effects on the resonance frequency. For instance, gold nanoparticles can readily adsorb protein molecules onto their surfaces, causing a shift of the resonance frequency into near infrared (IR) regime (the wavelength is between ~800 and 2500 nm) [3]. The transmittance of IR radiation in most soft tissues is high [4]. For instance, the absorption coefficient of breast tissue for IR radiation with a wavelength between 700 and 900 nm is very low (0.022–0.075 mm^{-1}) [5]. Therefore, the transmitted intensity is one-tenth of the incident intensity even for a large tissue thickness of about 30–100 mm. Due to the high degree of transparency of soft tissues to IR radiation, the absorption of IR photons by the biocompatible Au particles enables their application in cancer diagnosis [1,6–8]. Gold nanoparticles absorbing IR radiation also act as thermal heating resources, thereby killing the cancer cells locally. This feature of gold nanoparticles offers a new way of non-toxic

* Corresponding author. Tel.: +36 1 372 2876; fax: +36 1 372 2811.
E-mail addresses: gubicza@metal.elte.hu, jeno.gubicza@gmail.com (J. Gubicza).

0254-0584/$ – see front matter © 2013 Elsevier B.V. All rights reserved.
http://dx.doi.org/10.1016/j.matchemphys.2013.01.012

cancer treatment [9,10]. When coated with specific antibodies, the Au nanocrystals can be used to probe the presence and position of antigens on cell surfaces as well as to potentially deliver therapeutic agents selectively. For instance, cetyltrimethylammonium bromide (CTAB) coated gold nanoparticles has been successfully applied in breast cancer diagnosis [11]. The key features of CTAB as a surfactant are (i) its high water-solubility, (ii) its bromide counterions which can chemisorb on metal surfaces, (iii) its large headgroup that helps to direct which face of the crystal grows, and (iv) its long tail to make a stable bilayer on the metal surface [12]. Due to these features, CTAB can effectively stabilize the small size of gold crystals, but it also plays a very important role in controlling the shape of nanoparticles [9,12,13]. In this study, we show that there is an evolution of the size and shape of CTAB-coated gold nanoparticles during long-time aging which is mainly caused by Ostwald ripening, however, fusion of particles also occurs. A detailed investigation of the shape of the grown nanoparticles is also presented and the factors influencing the morphology are discussed.

2. Material and methods

CTAB-coated gold nanoparticles were prepared by seeding method. For the synthesis, CTAB, $HAuCl_6$ (Auric acid 99.99%), $NaBH_4$ (sodium borohydrate 99%) and Ascorbic acid were purchased from Merck KGaA, Darmstadt, Germany. First, 0.9 ml $NaBH_4$ 0.02 M was used to reduce 5 ml $HAuCl_4$ 1 M in 5 ml CTAB 1.5 M in order to obtain solution containing red brown seed Au particles. This seed solution was ready after 2–5 h processing. Then, the grow solution was created by adding 2.4 ml Ascorbic acid 0.02 M to 70 ml $HAuCl_4$ 1 M in CTAB 1 M in order to reduce Au^{3+} to Au^{+} ion. Finally, 0.5 ml seed solution was added to the grow solution leading to the slow change of color of the solution to red, indicating the formation of gold nanoparticles. The solution reached a stable state after storage for 12 h, and then it was washed with distillated water several times by centrifugation at 9000 rpm. The final solution was clean CTAB coated gold nanoparticles soluted in distilled water.

The particles' morphology was examined using Philips CM-20 and JEOL 3010 transmission electron microscopes (TEM) operating at 200 kV and 300 kV, respectively. The lattice defects were studied by X-ray line profile analysis. The measurement of the X-ray diffraction pattern was performed by a Philips Xpert powder diffractometer with CuKα radiation ($\lambda = 0.15418$ nm) and a pyrolithic graphite secondary monochromator. The line profiles were evaluated using the Convolutional Multiple Whole Profile (CMWP) fitting procedure [14]. In this method, the diffraction pattern is fitted by the sum of a background spline and the convolution of the instrumental pattern and the theoretical line profiles related to the crystallite size, dislocations and twin faults. The instrumental pattern was measured on a NIST SRM660a LaB_6 peak profile standard material. This method gives the crystallite size, the dislocation density and the twin boundary frequency with good statistics, where the twin boundary frequency is defined as the fraction of twin boundaries among the {111} lattice planes.

3. Results and discussion

The size of the as-processed spherical nanoparticles was between 2 and 5 nm as it is shown in the TEM image of Fig. 1a. The Au-CTAB nanoparticles were soluted and stored in distilled water at room temperature. After storage for one year, nanoparticles taken from the solution were investigated by TEM, revealing a particle coarsening as shown in Fig. 1b. The size of the coarsened nanoparticles is between 15 and 40 nm (the average size is 25 nm) and there is a large variety in their shapes: spheres, regular shapes with two-, three-, five- or six-fold symmetry are observed.

Fig. 2 shows magnified view of particles with regular shapes. The nanoparticles exhibiting three- and five-fold symmetries are triangular plates and decahedrons denoted by TP and D in Fig. 2a, respectively. A five-fold twinned, decahedral nanoparticle can be considered as an assembly of five single-crystal tetrahedral units sharing a common edge. Each tetrahedron is separated from its two neighbors by twin boundaries on {111} planes [3]. Since the theoretical angle between two {111} planes of a tetrahedron is 70.53°, five tetrahedrons joined with {111} twin planes will leave a gap of 7.35°, therefore after joining the tetrahedra, large elastic stresses are developed. This stress field can be described as the stress field of a disclination [15] which can be released by formation of dislocations. It has been shown that decahedral face centered cubic (fcc) nanoparticles did not develop through assembling of tetrahedra formed separately but rather produced via the stepwise growth of tetrahedral units on the {111} facets of intermediate species [16]. It has been also revealed that another route of this growth mechanism may result in icosahedron particles comprising twenty tetrahedrons. Although, in the present study perfect icosahedrons were not found among the inspected nanoparticles, intermediates of icosahedral particles which arise from a combination of ten tetrahedral units (deca-tetrahedra) were observed. For instance, the particle with six-fold symmetry in Fig. 2b is a deca-tetrahedron (denoted by DT) where the six triangular faces are the {111} facets of six tetrahedra from the ten units building up the particle. These tetrahedra are separated by twin boundaries. Both decahedron and

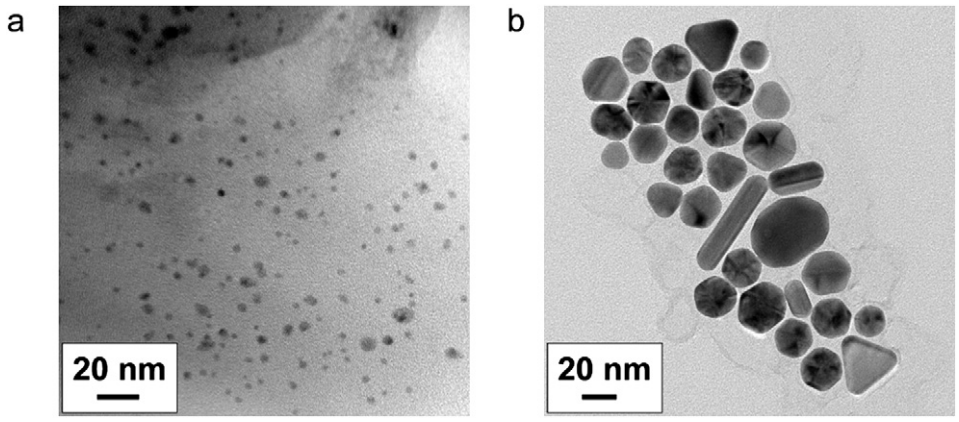

Fig. 1. TEM images obtained on Au-CTAB nanoparticles. a) immediately after production the size of the spherical Au nanoparticles was 2–5 nm, b) after one year of storage the gold particles grew to about 25 nm and exhibited different shapes.

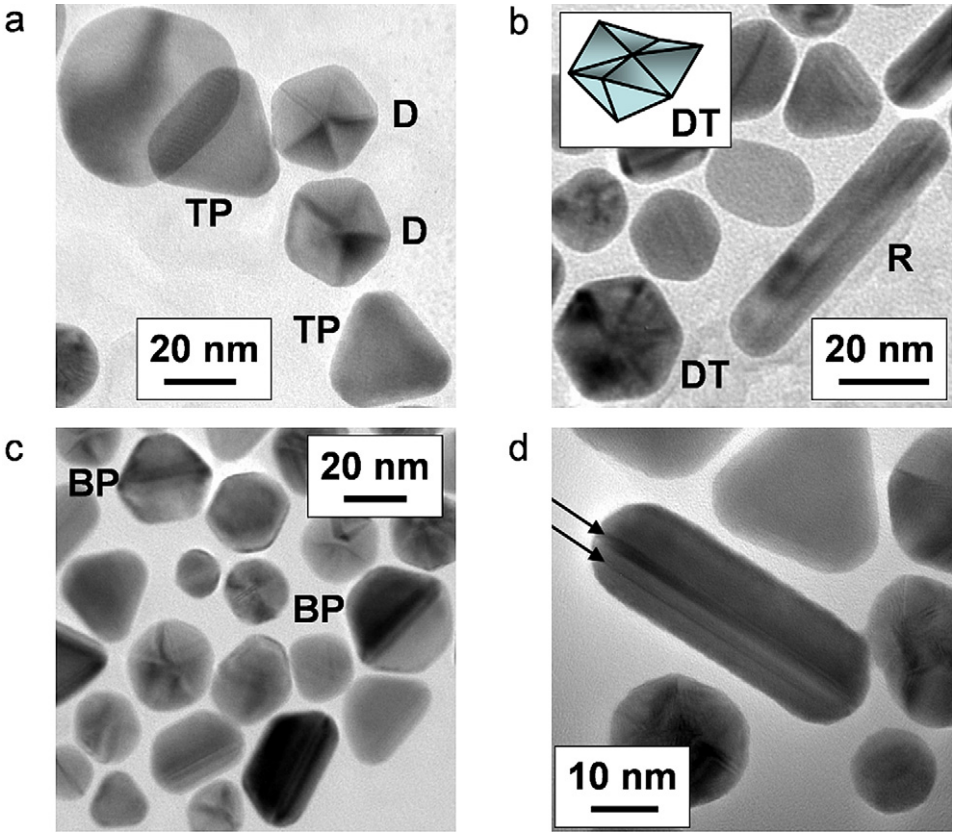

Fig. 2. TEM images showing the different types nanoparticles with regular morphology after one year of storage. a) Decahedron (D) and triangular plate (TP). b) Deca-tetrahedron (DT) and rod (R). The inset shows a schematic drawing of the three dimensional morphology of a deca-tetrahedron. c) Bipyramid (BP). d) The arrow indicates that the twin boundaries in a rod are lying parallel to its longitudinal axis.

icosahedron are thermodynamically favorable shape of Au and Ag nanocrystals since they are enclosed by very low energy {111} facets [16]. In general, in fcc nanocrystals the low-index crystallographic facets have the smallest specific surface energies (e.g. {111} and {100}) therefore usually they encase the nanocrystals [17]. Since {111} facets have the lowest energy [3] and the twin fault energy is also very low for Au and Ag [18], the free energies of twinned decahedron and icosahedron nanocrystals are lower than that of a single crystal Wulff polyhedron (a truncated octahedron enclosed by a mix of {111} and {100} facets). It is noted that our Au particles have rounded vertices, suggesting that the total surface energy of this morphology is lower than that for the nanocrystals with perfect regular shape due to the smaller total surface area in the former case.

Besides the thermodynamical viewpoint, the kinetics of crystal growth can also influence the shape of Au nanoparticles [19]. When the initial nanocrystal contains a stacking fault, the Au atoms add preferentially to the vicinity of the fault, hereby yielding a fast crystal growth parallel to the stacking fault [3]. Finally, a trigonal thin plate will form with the top and bottom faces being {111} facets [20,21]. The side surfaces are usually also {111} facets. It is emphasized that the growing of plate-like nanocrystals is never favored in terms of thermodynamics. The formation of triangular plates during aging of Au-CTAB sample is proved by the TEM image in Fig. 2a. When the initial crystal is singly twinned, then it will most probably grow into right-bipyramid which is a nanocrystal consisting of two right tetrahedrons symmetrically placed base-to-base and enclosed by {100} facets [22]. Fig. 2c shows some bipyramids denoted as BP.

The presence of a capping agent (e.g. CTAB) on the surface of nanocrystals can also influence the shape of the growing particles since the binding affinity of the capping agent can be different for the various crystal facets [3]. The strong binding of the capping agent to a particular facet can effectively hinder the addition of atoms, therefore the adatoms rather join other facets and the crystal will grow perpendicular to the latter faces. As a consequence, the facets with a lower addition rate will occupy more space on the surface of the nanoparticle. For example, bromide ions in CTAB bind most strongly to the {100} facets, therefore Au atoms will add preferentially to the poorly passivated {111} facets. Then, these adatoms migrate to the face edges, resulting in an elongation of the {100} facets and a formation of rods or beams [2]. Some rods in the present Au-CTAB specimen are shown in Fig. 2b and d. The diameter and the length of the rods are 10–20 and 25–110 nm, respectively, while the aspect ratio varies between 2 and 9. It has been shown that similar rods can grow from both single twinned bipyramids [23] and multiply twinned decahedrons [2,17,24].

The evolution of the particle size and morphology during storage is most probably initiated by a reduction in coverage of the particles' surfaces by CTAB. This capping agent stabilized the shape of the initial nanocrystals for a while, however, their degradation or gradual release into the solution enables the dissolution of the smallest gold nanoparticles and the growth of the larger particles, similar to Ostwald ripening. In a recent study [25], Ostwald ripening of CTAB-stabilized gold nanoparticles has been reported during seven days storage in hydrogen peroxide (H_2O_2) at room temperature. In that case, H_2O_2 redox induced simultaneous dissolution and growth of gold nanoparticles and bromide (Br^-) from CTAB helped to form $AuBr^{2-}$ in aqueous solution at room temperature. However, in the present case the TEM images in Fig. 3 reveal that besides growth via atomic addition, the nanoparticles can directly merge into larger objects via agglomeration. For instance,

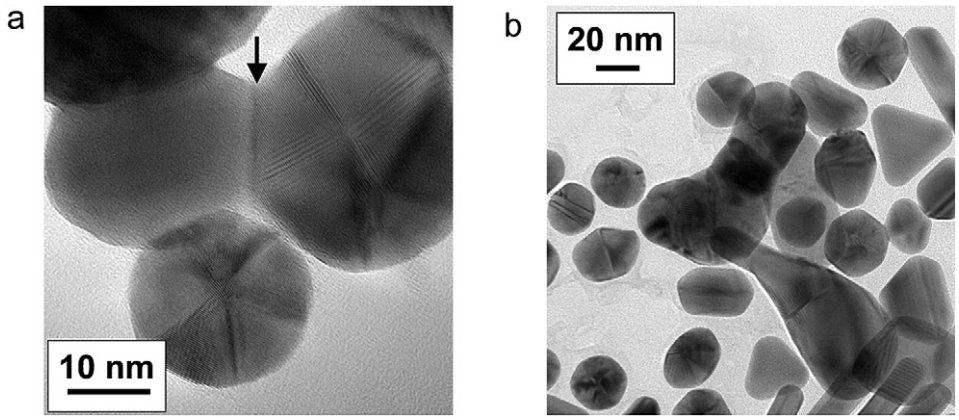

Fig. 3. TEM images of fused Au particles after storing them for one year. a) The arrow indicates the joint surface of two fused nanoparticles. b) The two large objects seem to be formed by the coalescence of several nanoparticles.

Fig. 3a shows two fused particles where the arrow indicates the joint surface. At the same time, in Fig. 3b the two large objects with irregular shapes seem to be formed from more than two particles and/or rods. It should be noted that other studies have also reported the change of the shape of Ag and Pd nanocrystals during their storage at room temperature [21,26]. In the case of Ag nanoparticles both photoinduced ripening [27] and coalescence during production by reduction [28] were also observed.

Our TEM images reveal that there is a very high density of twin boundaries in the Au nanoparticles stored for one year. These twin boundaries separate the tetrahedral units in the decahedra, decatetrahedra and bipyramids. The twin boundaries in the rods are lying parallel to the long axis. In order to characterize the frequency of twin boundaries quantitatively, X-ray line profile analysis was performed on Au nanoparticles. The Full Width at Half Maximum (FWHM) of the X-ray diffraction peaks as a function of the length of the diffraction vector ($g = 2\sin\theta/\lambda$, where θ and λ are the diffraction angle and the wavelength of X-rays, respectively) is plotted in Fig. 4a (Williamson-Hall plot). Since the majority of nanoparticles have equiaxed shape, therefore the much larger broadening of (200) and (400) reflections compared to other peaks is a fingerprint of the very high amount of twin boundaries [29].

The twin boundary frequency was determined by fitting the experimental diffraction pattern by the Convolutional Multiple Whole Profile (CMWP) method [14]. The measured and the fitted X-ray diffraction patterns are shown in Fig. 4b. The CMWP evaluation gives 5.3 ± 0.6% for the twin boundary frequency, which means that every twentieth {111} plane is a twin fault. Taking into account that the distance between the neighboring {111} planes in Au is $d_{111} = 0.235$ nm, the twin boundary frequency (β) can be transformed into a mean twin-spacing as $100 \cdot d_{111}/\beta$. For the present gold nanoparticles the mean twin-spacing obtained by X-ray line profile analysis is 4.4 nm which is in accordance with the TEM observations. The mean crystallite size ($\langle x \rangle$) obtained from the pattern fitting is 25 ± 3 nm which is in good correlation with the average particle size obtained by TEM. Fig. 4a also reveals that the broadening of the higher order peak in a harmonic reflection pair is larger (compare (200) and (400) or (111) and (222) reflection pairs), which indicates lattice strain inside the nanoparticles. The present X-ray line profile analysis is based on a microstructural model, in which the source of lattice strains is assumed to be dislocations. The dislocation density (ρ) obtained from the pattern fitting is $1.4 \pm 0.2 \times 10^{16}$ m^{-2}. It should be noted, however, that in the investigated gold nanoparticles in addition to dislocations there may be other sources of elastic lattice strains such as the particles' surface tension or disclinations in decahedrons. Therefore, it is reasonable to convert the experimentally obtained dislocation density into an average root mean square strain using the following formula [30]

$$\left\langle \varepsilon^2 \right\rangle^{1/2} = \left(\frac{\rho \overline{C} b^2}{4\pi} \ln\left(\frac{R_e}{L}\right) \right)^{1/2}, \quad (1)$$

where $\overline{C}$ is the average dislocation contrast factor ($\overline{C} = 0.31$ for reflection (200)), b is the magnitude of the Burgers-vector ($b = 0.29$ nm) and R_e is the outer cut-off radius of dislocations ($R_e = 5.4$ nm as obtained by X-ray line profile analysis), respectively, and L is the Fourier-length ($L = 2.9$ nm was selected as the mean of

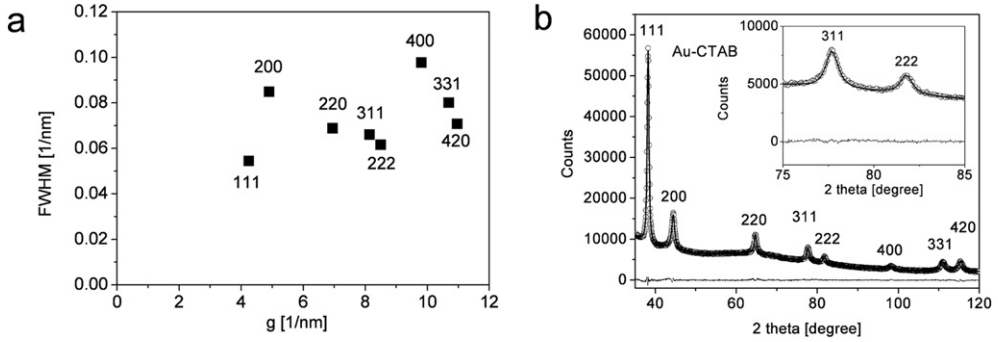

Fig. 4. X-ray line profile analysis on the aged gold nanoparticles. a) Williamson-Hall plot of the full width at half maximum (FWHM) of the X-ray diffraction peaks as a function of the length of the diffraction vector (g) for Au nanoparticles after one year of storage. b) The fitting of the X-ray diffraction pattern for Au nanoparticles stored for one year: The open circles and the solid line represent the measured data and the fitted curves, respectively. The difference between the measured and fitted patterns is also shown at the bottom of the figure.

the shortest (b) and longest (R_e) reasonable distances around dislocations). The average elastic strain calculated from this formula is $\langle \varepsilon^2 \rangle^{1/2} = 0.4\,\%$.

4. Conclusion

In conclusion, we have demonstrated that the long-time aging of Au nanoparticles covered by CTAB with the size of 2–5 nm yielded a considerable particle growth to about 25 nm and a formation of regular shapes such as decahedra, deca-tetrahedra, bipyramids, triangular plates and rods. The particles' morphology suggests that the main mechanism of this evolution is an Ostwald ripening, although fusion of particles was also observed. A very high density of twin boundaries was detected inside the particles which also influences the shape of the growing crystals. The aging has a potential in providing the desired shape and size of nanoparticles, if the evolution processes are controlled appropriately.

Acknowledgments

This work was supported by the Hungarian Scientific Research Fund, OTKA, No. K-81360 and by Vietnam Ministry of Science and Technology, Project 2/2010/HD-NCCBUD. The European Union and the European Social Fund have provided financial support to this project under Grant Agreement No. TÁMOP 4.2.1./B-09/1/KMR-2010-0003.

References

[1] P.K. Jain, I.H. El-Sayed, M.A. El-Sayed, Nano Today 2 (2007) 18–29.
[2] C.J. Murphy, T.K. Sau, A.M. Gole, C.J. Orendorff, J. Gao, L. Gou, S.E. Hunyadi, T. Li, J. Phys. Chem. B 109 (2005) 13857–13870.
[3] Y. Xia, Y. Xiong, B. Lim, S.E. Skrabalak, Angew. Chem. Int. Ed. 48 (2009) 60–103.
[4] C.L. Tsai, J.C. Chen, W.J. Wan, J. Med. Bio. Eng. 21 (2001) 7–14.
[5] V.G. Peters, D.R. Wyman, M.S. Patterson, G.L. Frank, Phys. Med. Biol. 35 (1990) 1317–1334.
[6] C.J. Murphy, A.M. Gole, J.W. Stone, P.N. Sisco, A.M. Alkilany, E.C. Goldsmith, S.C. Baxter, Acc. Chem. Res. 41 (2008) 1721–1730.
[7] M.V. Yezhelyev, X. Gao, Y. Xing, A. Al-Hajj, S. Nie, R.M.O. 'Regan, Lancet Oncol. 7 (2006) 657–667.
[8] M. Ferrari, Nat. Rev. Cancer 5 (2005) 161–171.
[9] X. Huang, I.H. El-Sayed, M.A. El-Sayed, J. Am. Chem. Soc. 128 (2006) 2115–2120.
[10] E.B. Dickerson, E.C. Dreaden, X. Huang, I.H. El-Sayed, H. Chu, S. Pushpanketh, J.F. McDonald, M.A. El-Sayed, Cancer Lett. 269 (2008) 57–66.
[11] L.M. Quynh, T.Q. Tuan, N.H. Luong, N.N. Long, N.H. Hai, T.T.T. Thoa, N.T.V. Anh, P.T. Nghia, e–J. Surf. Sci. Nanotech 9 (2011) 544–547.
[12] N.N. Long, L.V. Vu, C.D. Kiem, S.C. Doanh, C.T. Nguyet, P.T. Hang, N.D. Thien, L.M. Quynh, J. Phys. Conf. Ser. 187 (2009) 012026.
[13] R. Narayanan, R.J. Lipert, M.D. Porter, Anal. Chem. 80 (2008) 2265–2271.
[14] G. Ribárik, J. Gubicza, T. Ungár, Mater. Sci. Eng. A 387–389 (2004) 343–347.
[15] V.G. Gryaznov, Cryst. Res. Technol. 34 (1999) 1091–1119.
[16] M. Tsuji, M. Ogino, R. Matsuo, H. Kumagae, S. Hikino, T. Kim, S.-H. Yoon, Cryst. Growth Des. 10 (2010) 296–301.
[17] A.R. Tao, S. Habas, P. Yang, Small 4 (2008) 310–325.
[18] J.P. Hirth, J. Lothe, Theory of Dislocations, Wiley, New York, 1982.
[19] Y. Sun, Y. Xia, Science 298 (2002) 2176–2179.
[20] V. Germain, J. Li, D. Ingert, Z.L. Wang, M.P. Pileni, J. Phys. Chem. B 107 (2003) 8717–8720.
[21] Y. Xiong, A.R. Siekkinen, J. Wang, Y. Yin, M.J. Kim, Y. Xia, J. Mater. Chem. 17 (2007) 2600–2602.
[22] Y. Xiong, H. Cai, Y. Yin, Y. Xia, Chem. Phys. Lett. 440 (2007) 273–278.
[23] B.J. Wiley, Nano Lett. 6 (2006) 2273–2278.
[24] Y. Xiong, Y. Xia, Adv. Mater. 19 (2007) 3385–3391.
[25] E. Jang, E.-K. Lim, J. Choi, J. Park, Y.-J. Huh, J.-S. Suh, Y.-M. Huh, S. Haam, Cryst. Growth Des. 12 (2012) 37–39.
[26] Y. Xiong, H. Cai, B.J. Wiley, J. Wang, M.J. Kim, Y. Xia, J. Am. Chem. Soc. 129 (2007) 3665–3675.
[27] R. Jin, Y.W. Cao, C.A. Mirkin, K.L. Kelly, G.C. Schatz, J.G. Zheng, Science 294 (2001) 1901–1903.
[28] Á. Bajáki, J. Lábár, Á. Csanády, O. Geszti, H. Hargitai, F.H. Kármán, Mater. Sci. Forum 659 (2010) 115–120.
[29] J. Gubicza, S. Nauyoks, L. Balogh, J. Lábár, T.W. Zerda, T. Ungár, J. Mater. Res. 22 (2007) 1314–1321.
[30] A. Zhilyaev, J. Gubicza, G. Nurislamova, Á. Révész, S. Surinach, M.D. Baró, T. Ungár, Phys. Stat. Sol.(a) 198 (2003) 263–271.